Optimisation of cold-formed steel beams for best seismic performance in bolted moment connections

Seyed Mohammad Mojtabaei[1], Iman Hajirasouliha[1], and Jun Ye[2]*

[1] *Department of Civil Engineering and Structural Engineering, The University of Sheffield, Sheffield S1 3JD, UK*

[2] *Department of Civil and Environmental Engineering, Imperial College London, London SW7 2AZ, UK*

* Corresponding author, E-mail: j.ye13@imperial.ac.uk

Abstract

Typical thin-walled cold-formed steel (CFS) elements and connections used in portal frames are not generally suitable for moment-resisting frames in high seismic regions due to their low ductility and energy dissipation capacity and inherited susceptibility to local/global instabilities. This study aims to improve the seismic performance of CFS moment-resisting frames by developing a methodology to obtain more efficient bolted moment connections using optimised CFS beams with enhanced non-linear post-buckling behaviour. By taking into account material non-linearity and geometrical imperfection effects, the detailed Finite Element (FE) models of a typical CFS bolted moment connection is developed using ABAQUS software, and then validated based on experimental cyclic test results. Particle Swarm Optimisation (PSO) algorithm is linked to GMNIA ABAQUS FE analysis to optimise CFS bolted moment connections based on either energy dissipation capacity or ductility. To demonstrate the efficiency of the method, connections with five different beam cross-sectional shapes are optimised, and the results are compared with a standard CFS channel section used as a benchmark. The relative dimensions of the cross-sections, the inclination of the lip stiffeners, and the location of triangular intermediate stiffeners are selected as main design variables. To provide practical beam cross-sections, the plate slenderness limit values defined by Eurocode 3 (EC3) along with a range of manufacturing limitations are imposed as design constraints in the optimisation process. It is shown that, for a given plate width and thickness, the proposed optimisation framework results in a considerable (up to 195%) improvement in the energy dissipation capacity and ductility of the CFS bolted moment connections.

Keywords: Cold-formed steel (CFS); bolted moment connection; Particle Swarm Optimisation (PSO); Finite Element (FE) analysis; energy dissipation; ductility

1 Introduction

Cold-formed steel (CFS) members are manufactured by bending or press-breaking thin-walled steel coils at ambient temperature to the desired cross-sectional shapes. The light-weight CFS structural elements can provide a high strength-to-weight ratio, more flexible member profiles compared to hot-rolled sections, and also facilitate onsite manufacturing and installation [1, 2]. Previous studies indicated that, compared to conventional CFS shear wall panel systems, moment-resisting frames with CFS members generally can provide more efficient design solutions in terms of seismic characteristics such as ductility and energy dissipation capacity [3, 4]. Currently, the applications of CFS moment-resisting systems are mainly limited to portal frames and industrial platforms where higher mobility and space-planning flexibility is required. However, CFS elements and conventional connections are not considered to be suitable for moment-resisting frames in high seismic regions due to their susceptibility to local and global instabilities which reduces their ductility and energy dissipation capacity [5, 6].

In general, beam-to-column connections play a key role in the global behaviour, strength, and seismic characteristics of moment-resisting frames under seismic excitations [7-10]. Several studies have experimentally and analytically investigated the structural performance of apex and eaves CFS connections under monotonic loads (e.g. [11-21]). It was concluded that the local buckling of CFS beam close to connection zone was normally identified as a dominant failure mode, while it was shown that bolt-group size can have a significant effect on the flexural strength of the connections. The results of experimental cyclic tests on CFS bolted moment connections indicate that a rigid behaviour (based on Eurocode [22] definition) can be obtained if the connections are designed properly [3, 23]. Bučmys et al. [24] presented an analytical approach to determine the rotational stiffness of CFS bolted moment connections based on the component method stipulated in Eurocode 3 [25]. In other relevant studies, Rinchen and Rasmussen [16] and Phan et al. [19] developed design approaches for the flexural

strength of bolted connections by considering the effects of bimoment. The design aspects of the CFS bolted moment connections were further explored by Mojtabaei et al. [20], who attributed premature failure in the web of the cross-section to the shear lag effect.

While using multiple plate stiffeners in the connection zone can postpone the failure of the CFS beam and ultimately lead to a considerable increase in the ductility of the connection [26], this may not be a practical solution due to complexity of the required detailing. More recent studies by Ye et al. [27] demonstrated that beam cross-sectional shapes and slenderness, gusset plate thicknesses, and bolt distribution can also significantly (up to 250%) improve the seismic performance of bolted moment connections. In a follow-up study, it was shown that incorporating bolting friction slip mechanism can result in up to 200% higher dissipated energy, ductility and damping coefficient of the connections particularly for CFS beams with thinner plates (Eurocode classes 3 and 4) [28]. Sato and Uang [29] also demonstrated that the ductility of CFS special bolted moment frames defined by AISI S110 standard [30] can be enhanced through bearing action and slippage of the bolts.

In general, CFS elements can be optimised by changing the relative dimensions of their cross-sections [31, 32]. There are several studies, in particular, on the optimum design of CFS beam elements to maximise their ultimate capacity [33-35], energy dissipation capacity [36] and flexural stiffness [37]. However, the presence of the bolts in CFS bolted moment connections can change the flexural performance of the system due to the effects of bi-moment [11, 16, 19], shear lag [20] and bolt-web interactions [27, 28]. Currently, there is no study on the optimisation of CFS bolted moment connections incorporating the bolt effects. This is especially important since the seismic performance of multi-storey CFS moment-resisting systems is directly affected by the behaviour of their connections.

This paper aims to develop, for the first time, a framework for shape optimisation of CFS bolted moment connections to maximise their seismic characteristics including energy dissipation capacity and ductility by incorporating the bolt effects. Detailed FE models of bolted moment connections are developed in ABAQUS [38] by taking into account material nonlinearity and geometrical imperfections,

while the adopted modelling technique is validated against available experimental test results. Five different CFS beam cross-sectional shapes are selected and their relative dimensions, location of intermediate stiffeners, and the inclination of the lip stiffeners are considered as key design variables. Optimisation process is done by using a MATLAB code [39] which is developed to link Particle Swarm Optimisation (PSO) [40] to the validated FE models in ABAQUS [38]. While all the previous studies optimised the behaviour of CFS element under monotonic loading, in this study the optimisation process is conducted under both monotonic and cyclic loading conditions to take into account the stiffness and strength degradation effects. The efficiency of the obtained optimised design solutions compared to standard sections is then demonstrated under cyclic loading condition. Finally, the results are used to investigate the effect of hysteretic loops on the seismic performance of the optimised and conventional bolted moment connections.

2 Seismic design provisions for CFS bolted connections

This section presents a brief introduction of the relevant seismic design codes including European, American and Australia/New Zealand specifications. Furthermore, the application of these codes is also discussed for the specific type of connections selected in this study where the connection is manufactured by bolting the webs of the back-to-back channel section to the gusset plate while the flanges left unconnected.

2.1 European code

The scope of European design guidelines for the earthquake-resistant steel structures (i.e. Eurocode 8) [41] is limited to the hot-rolled steel and generally cannot be applicable for CFS structures. However, the rigidity of the steel connections can be assessed based on the provisions of EN 1993-1-8 (i.e. Eurocode 3 Part 1-8) [25]. According to EN 1993-1-8, the moment-rotation relationship is first derived, and the initial stiffness ($S_{j,ini}$) is then defined as the slope of the moment-rotation curve at a value of $2/3 \times M_{j,R}$, where ($M_{j,R}$) is the moment resistance of the connection. Finally, the connection is categorised as either rigid, semi-rigid or pinned by comparing the initial stiffness ($S_{j,ini}$) with the predetermined boundaries. For a rigid connection, the initial stiffness has to be greater or equal to

$k_b \times E \times I_b / L_b$, where k_b=25 for no bracing system, E is the elastic modulus, I_b is the second moment of area of the beam, and L_b is the beam span between the centres of the adjacent columns. The connection is classified as pinned if the initial stiffness is smaller or equal to $0.5 \times E \times I_b / L_b$. For intermediate values between the two boundaries, the connection falls into the semi-rigid class. These general requirements for the assessment of rigidity can be applied for the particular type of connections discussed in the current study. According to the previous studies by Sabbagh et al. [3] and Ye et al. [27] this type of connections was mainly identified as rigid connections.

2.2 American code

North American Specifications for Seismic Design of Cold-Formed Steel Structural Systems (AISI S400-15) [42] represents a basic configuration for a special bolted moment frame using Hollow Structural Section (HSS) uprights and relatively stocky CFS channel beams with a specially detailed bolt group at the beam-to-column connection. The AISI Specifications for bolted connections in the seismic area are mainly based on the experimental work conducted by Uang et al. [43]. While the AISI proposed system can develop significant ductility and satisfy the Special Moment Frame (SMF) requirements stipulated by AISC 341-16 [44] (i.e. drift capacity larger than 0.04 radians), the AISI imposed several limitations, as an instance, the application of this system is limited to a single storey mezzanine and residential structures. The other limitations can be found in Clause E4.4.1 of the AISI S400-15 [42]. It should be noted that according to the studies conducted by Mojtabaei et al. [19, 20, 45] the load transfer mechanism of the selected type of connections in this study is fundamentally different from the connections presented by AISI [42] due to the effect of shear lag/bimoment. Therefore, while the general specifications stipulated by AISI [42] cannot be directly applicable for this type of connections, the general requirements imposed by AISC [44] for the SMF are used in this study (see Section 4).

2.3 Australia and New Zealand code

Australian/New Zealand Standard for CFS structures (AS/NZS 4600:2018) [46] provides two different specifications for Australia and New Zealand. For Australia, if CFS members are used as the primary

earthquake resistance element, then the structural response factor (R_f) shall be less than or equal to 2. On the other hand, for New Zealand the value of the structural ductility factor (μ) should be between 1 and 4, depending on the conditions specified in clause 1.6.4.2.2 of AS/NZS 4600:2018 [46].

3 Modelling of tested bolted moment connections

Typical bolted moment connections aimed in this research consist of a column and a beam with back-to-back CFS channel sections connected by bolts, gusset plate, and column stiffeners as shown in Fig. 1. Sabbagh et al. [3] conducted several experimental tests on this type of CFS bolted moment connections at The University of Sheffield. The column stiffeners are used to prevent premature failure modes in the column to be consistent with the reference experimental tests [3]. The gusset plate passed through the back-to-back beam and column can transfer bending moment and shear force from the CFS beam to the column. More detailed information about the reference experimental programme can be found in [5]. In this study, the results of two tests, namely connections A1 and B1, are used as a benchmark to validate the FE models developed in ABAQUS software [38] as will be explained in the following subsection.
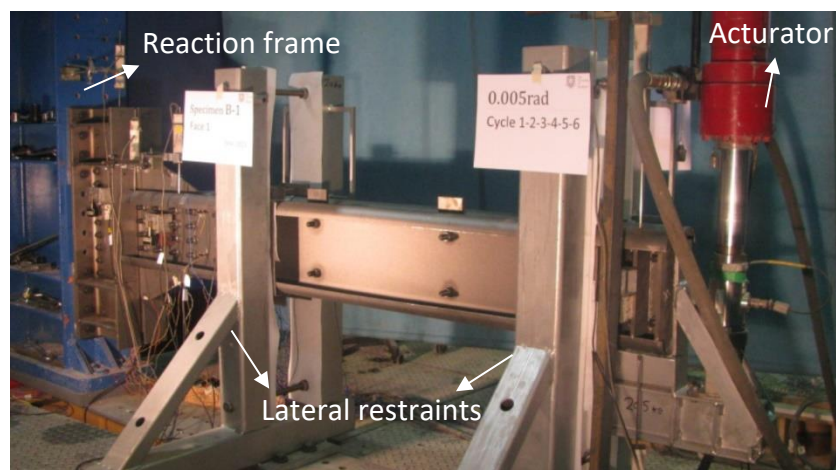
Fig. 1. Experimental test set-up of the bolted moment connections [5]

3.1 Material properties and element type

The measured stress-strain curves of the CFS elements obtained from the average of two coupon tests [5] are incorporated in the FE models (see Fig. 2). In this study, the material yield stress (σ_y), the

ultimate stress (σ_u) and module of elasticity (E) are taken equal to 313 MPa, 479 MPa and 210 GPa

for the connection A1, and 322 MPa, 479 MPa and 210 GPa for the connection B1, respectively. Since

it was reported that the analysis of post-failure of CFS bolted moment connections involves large

inelastic strains [3], the nominal (engineering) static stress-strain curve is converted to a true stress

and logarithmic plastic strain curve. The true stress σ_{true} and plastic true strain ε_{true}^{pl} required by

ABAQUS [38] are defined as:

$$\begin{cases} \sigma_{true} = \sigma(1 + \varepsilon) \\ \varepsilon_{true}^{pl} = \ln(1 + \varepsilon) - \dfrac{\sigma_{true}}{E} \end{cases} \tag{1}$$

where σ and ε represent the engineering stress and strain, respectively, and E is the module of

elasticity of the material.

The CFS connections are modelled using 8-node quadrilateral shell elements with reduced integration

and four nodal degrees of freedom (S8R). Following a sensitivity analysis, the mesh size providing

adequate accuracy with minimum computational time is selected to be 20 mm.
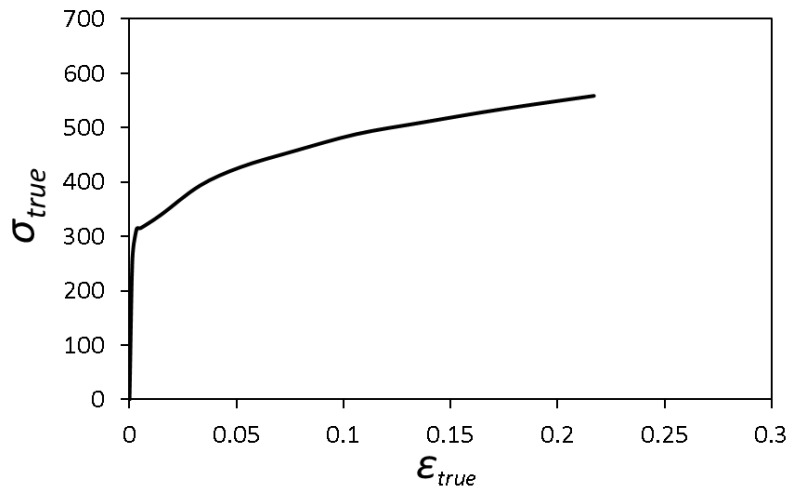
Fig. 2. True stress-strain curve used in the FE modelling of connection A1

3.2 bolt modelling

To model the bolt-group, the discrete structural "fastener" available in ABAQUS [38] is adopted. A

similar technique has been adopted by Usefi et al. [47] to model the behaviour of connections in CFS

wall panels. The discrete fasteners make use of attachment lines to create connectors for coupling

between the selected faces. To model the connector element, a "physical radius" (r) is defined to represent the bolt shank radius and simulate the interaction between the bolt and the nodes at the bolt hole perimeter. The displacement and rotation of each fastening point were coupled to the average displacement and rotation of the surface nodes within the radius of influence (r). The adopted method can accurately capture the stress concentrations around the nodes at the bolt positions and help to simulate more accurately the bearing work of the bolts. In this study, r is assumed to be half of the bolt shank. This modelling technique has been successfully applied in the modelling of CFS bolted moment connections [20, 45]. Considering that no bolt damage was observed in the reference experimental tests [3], the failure modes of the bolts were not considered in this study.

3.3 Imperfection

As can be seen in Fig. 1, to prevent global buckling of the beam specimens, lateral displacements were restrained in the x-direction in the experimental tests [3]. Therefore, either a distortional or a local geometrical imperfection was incorporated into the FE models, depending on which mode had the lower critical buckling resistance. The imperfection amplitude for the steel sheets with the plate thickness (t) less than 3 mm was defined as $0.34t$ and $0.94t$ for the local and distortional imperfection, respectively, as recommended by Schafer and Peköz [48]. For the elements with higher plate thicknesses, the imperfect magnitude was determined based on the work by Walker [49] :

$$\omega_d = 0.3t \sqrt{\frac{\sigma_{0.2\%}}{\sigma_{cr}}} = 0.3t\lambda_s \tag{2}$$

where $\sigma_{0.2\%}$ and σ_{cr} are 0.2% proof stress of the material and elastic local buckling stress, respectively; and λ_s is cross-sectional slenderness. The general shapes of beam cross-sections after incorporating geometrical imperfections were generated by using an eigenvalue elastic buckling analysis in ABAQUS [38], and were then scaled based on the calculated imperfection magnitudes.

3.4 Loading and boundary conditions

The boundary conditions in the FE models were imposed based on the test set-up used in the experiments [3] (see Fig. 3). The translational degrees of freedom U_X, U_Y and U_Z on the bottom, and U_X and U_Y on the top surface of the back-to-back channel column were restrained. The column stiffeners were also tied to the column surfaces to be consistent with the experimental test set-up. The nodes at the location of the interconnections along the length of the CFS beam were tied in the U_X, U_Y and U_Z directions by using "Tie" constraint in ABAQUS [38]. The out of plane movement of the CFS beam is restrained at the location of the lateral bracing system of the experimental test set-up.

Both monotonic and cyclic loads were applied incrementally by using the "STATIC GENERAL" method in the ABAQUS library, which can take into account the non-linear behaviour of the material and the stiffness degradation due to buckling. The static concentrated load was applied through a displacement at the beam end nodes, which were coupled to the centroid of the cross-section as shown in Fig. 3. The effects of large displacements were considered by using the nonlinear geometry parameter "NLGEOM". For cyclic analyses, the ANSI/AISC 341-16 [44] proposed loading regime shown in Fig. 4 was adopted.
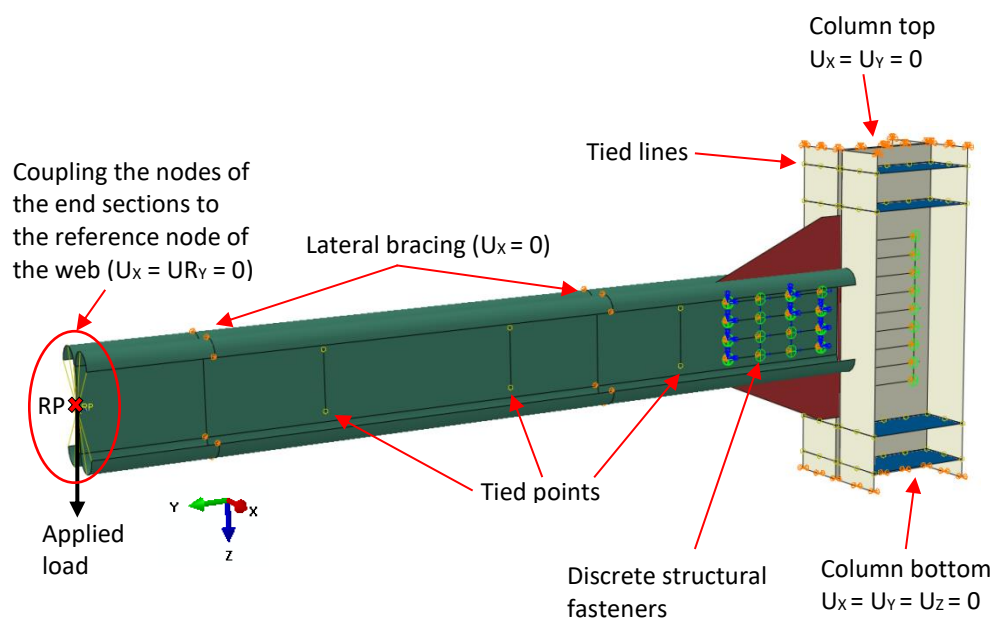
Fig. 3. Boundary conditions of the FE model for typical bolted moment connections
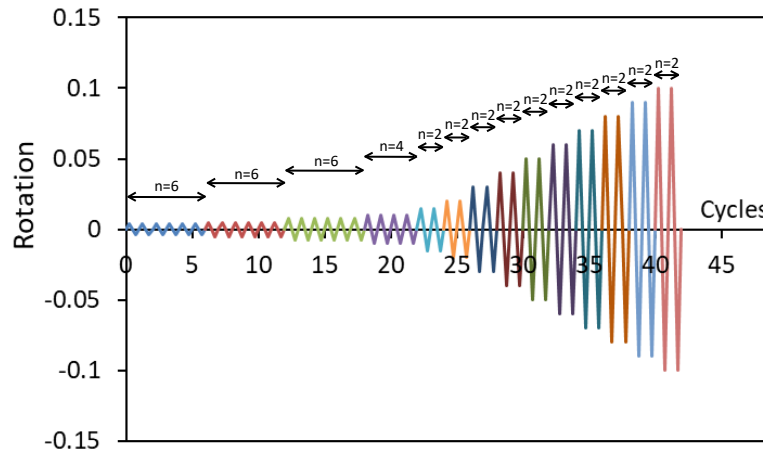
**Fig. 4.** Cyclic loading protocol in accordance with ANSI/AISC 341-16 [44] (n is the number of cycles)

3.5 FE modelling Validation

As mentioned before, the CFS bolted moment connections A1 and B1 tested by Sabbagh et al. [3] were used to validate the FE models developed in this study. Fig. 5 shows the moment-rotation curves scaled to the plastic moment of the CFS beam (M_p) obtained from the experimental tests (A1 and B1) and the corresponding detailed FE models under both cyclic and monotonic loads. The rotation of the connection was determined according to the ratio of beam tip displacement to the length of the beam up to the gusset plate. In general, it is shown that the FE models could simulate the behaviour of the connection tests A1 and B1 with a good level of accuracy over the whole loading range. While the initial stiffness of the tested connection perfectly matches with that obtained from the FE model, the maximum flexural capacities of the experiment and FE model reach 54.3 kN.m and 51.6 kN.m for the test A1, and 81.7 kN.m and 82.4 kN.m for the test B1, respectively. Besides, a comparison between the FE cyclic and monotonic results indicates that the initial stiffness and the maximum strength values are coincident. However, the results of the monotonic analyses slightly underestimated the stiffness degradation rate. The results of the experimental tests showed that the failure mode happened locally in the beam web close to the connection zone (see Figs. 6 (a) and 7 (a)). Similarly, the dominant failure of the CFS bolted moment connection under both monotonic and cyclic loads obtained from FE analysis generally started with the local buckling at beam webs followed by buckling of the compression flange, as shown in Figs. 6 (a) and 7 (b). These observations confirm the adequacy of the

adopted FE models in this study. It should be noted that the adopted FE method has been also verified against experimental results reported by Lim and Nethercot [11] in two recent publications by the authors [20, 45].
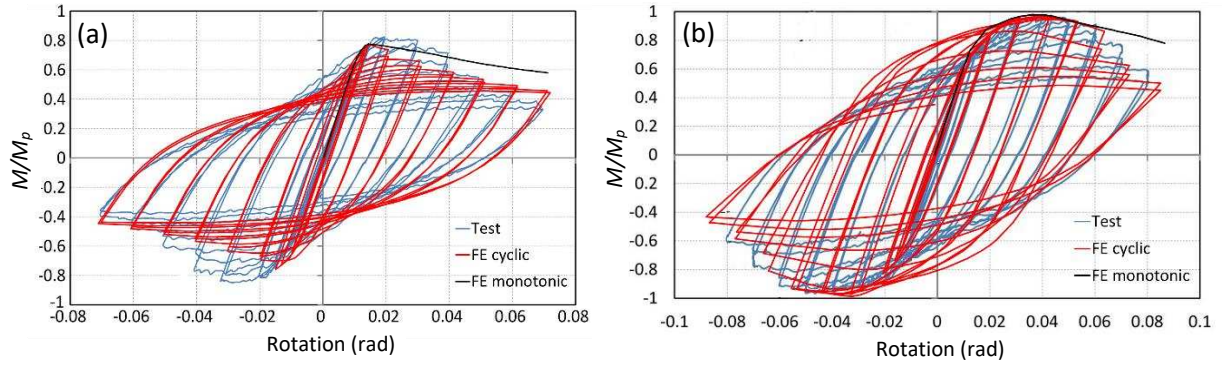
Fig. 5. Comparison between the results of tests and FE analyses of the connections: (a) A1 and (b) B1
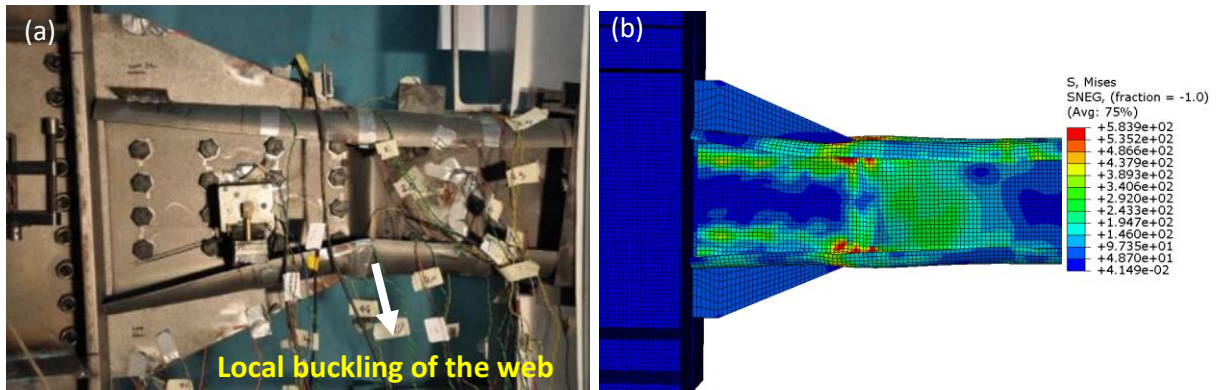
Fig. 6. Failure modes of the A1 CFS bolted moment connection under cyclic load: (a) test and (b) FE
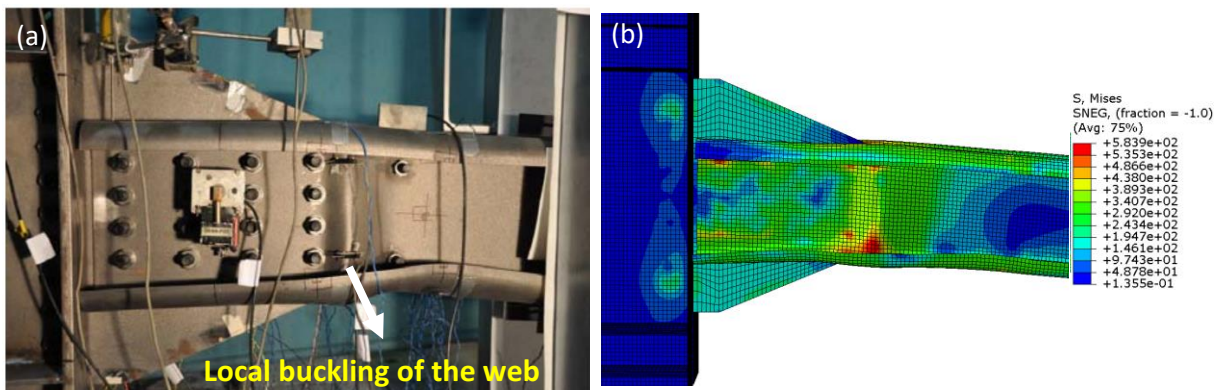
Fig. 7. Failure modes of the B1 CFS bolted moment connection under cyclic load: (a) test and (b) FE

4 Definition of seismic characteristics

Ductility and energy dissipation capacity are considered as key performance parameters for the seismic design of moment-resisting frames, where the structural components are expected to exceed their elastic limits in severe Earthquakes.

4.1 Energy dissipation

The earthquake-induced energy in CFS moment-resisting frames is mainly dissipated by their bolted moment connections through plastic deformation of the beam elements as well as bearing deformation of bolts against a steel plate. To estimate the plastic energy dissipation of the connections in ABAQUS, the following integration is used through the beam volume (V) and loading history (t):

$$E = \int_V \int_0^t \sigma_{ij}(\tau)\dot{\varepsilon}_{ij}^p \, d\tau dV \tag{3}$$

where $\sigma_{ij}(\tau)$ is the plastic stress tensor and $\dot{\varepsilon}_{ij}^p$ is the first derivative of plastic strain tensor with respect to time. In this study, the energy dissipation of CFS bolted moment connection is determined up to 4% (rad) inter-story drift ratio, which is in accordance with the AISC 341-16 [44] requirements for the Special Moment Frame (SMF), to provide a fair comparison between different cases.

4.2 Ductility ratio

The ductility ratio (μ) for the connections can be determined using the ratio of target rotation (θ_t) to yield rotation (θ_y) of an idealised bi-linear moment-rotation curve as the representative of the actual structural response of the system:

$$\mu = \frac{\theta_t}{\theta_y} \tag{4}$$

In this study, the idealised moment-rotation curve is determined using ASCE 41-17 [50] proposed method, in which an iterative graphical procedure is adopted to balance the areas below the actual and idealised curves up to the target rotation (θ_t). The yield rotation (θ_y) is obtained based on the condition that the first line segment intersects the actual envelope curve at 60% of the nominal yield moment (M_y), as shown in Fig. 8. The target rotation (θ_t) depends mainly on the expected performance from the connections. Generally, it is assumed that the target rotation is the maximum

12

rotation prior to a considerable fall in the strength of the system [51, 52]. In this study, the target rotation is considered as the rotation at which the flexural capacity of the connection is reduced by 20% as also recommended by ANSI/AISC 341-16 [44].
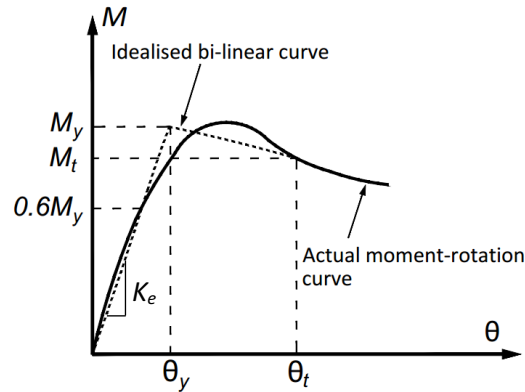
Fig. 8. Calculation of ductility based on ASCE's method [50]

To ensure the adopted FE models can predict the seismic characteristics of the CFS connections, the normalised flexural strength to plastic strength of the beam section, energy dissipation capacity and ductility of the tests A1 and B1 and the FE models are listed in Table 1. Considering the complex behaviour of CFS connections, the results in general confirm the acceptable accuracy of the FE predictions. It should be noted that the main purpose of this study is to compare the ductility and energy dissipation of the connections with optimum and standard sections. Therefore, the small error in the estimation of these values will not significantly affect the outcome.

Table 1. Comparison between the seismic characteristics of the connection tests A1 and B1 and the corresponding FE models

Connection		M_{max}/M_P	E (kJ)	μ
A1	Test	0.81	13.5	2.9
	FE model	0.77	12.8	3.2
B1	Test	0.91	19.2	3.7
	FE model	0.92	19.5	3.6

It should be noted that there is not a direct correlation between these two performance parameters. The energy dissipation is defined as the area below the moment-rotation curve while the ductility is

the ratio of ultimate rotation (or target rotation) to the yield rotation. Therefore, the connections with low yield rotation and small flexural capacity may lead to a high ductility but a low energy dissipation capacity. Therefore, in this study, both of these parameters are used as optimisation targets to improve the seismic performance of CFS connections.
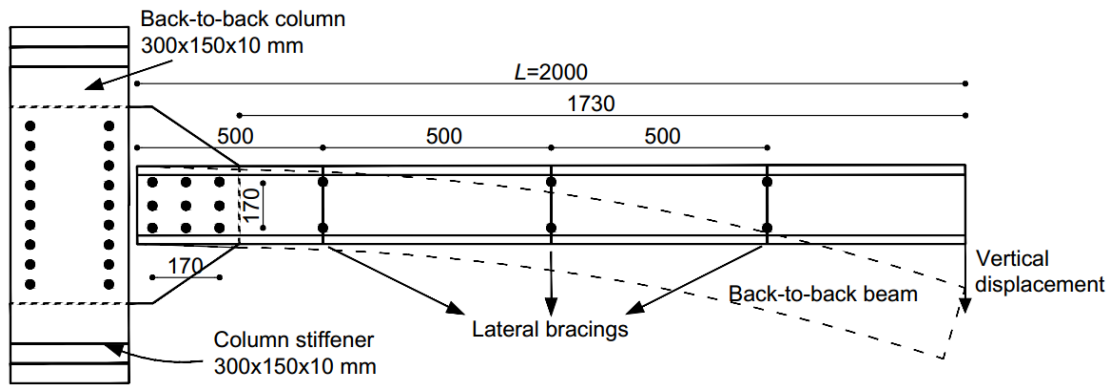
5 Connection optimisation

This section is aimed to find best design solutions for the bolted moment connections in terms of either energy dissipation capacity or ductility, as key seismic performance parameters, by optimising the cross-sectional shapes of the CFS beam element. The experimentally validated FE models of CFS bolted moment connections subjected to monotonic loading (discussed in Section 3) are used to simulate the non-linear response of the connections. A standard commercially available back-to-back lipped-channel section is taken as a benchmark to assess the efficiency of the optimised sections. Five different cross-sectional shapes are selected for the CFS beam element, including channel sections with inclined lips, rolled-in intermediate stiffeners in flange and web, and folded-flanges. Design constraints are imposed on plate slenderness and relative dimensions of the cross-sections according to Eurocode 3 [53, 54], while a range of manufacturing limitations are also considered as suggested by the industrial partner of this project (see Table 2).

It should be noted that optimisation of the connections under cyclic loading will be too computationally expensive to be practical, and therefore in this study, the connections are optimised under monotonic loading condition. However, it will be discussed in Section 8 that using monotonic or cyclic loading in the optimisation process leads to the same optimised design solution.

5.1 Problem formulation

Similar to the reference experimental test, a cantilever beam-to-column bolted connection loaded concentrically is selected for the optimisation, as shown in Fig. 9. The length of the CFS beam element L=2000 mm is considered to represent a mid-length contraflexure point in a typical moment-resisting frame with 4000 mm span subjected to lateral loading. The bolt-group size of 170×170 mm arrayed 3x3 is selected and kept constant during the optimisation process. To avoid global buckling of the CFS beam,

lateral restraints are placed at 500 mm spacing along the length of the beam. Other parameters and modelling techniques such as material properties, loading, element types, mesh size and bolt modelling are taken the same as the experimentally validated connection discussed in Section 3. To find the best design solution for the CFS beam cross-sections, bolted moment connections loaded monotonically in a displacement control manner are analysed in each iteration of the optimisation process. The moment-rotation ($M - \theta$) response of each connection is then calculated from the centre of failure (i.e. plastic hinge region), which is assumed to be located at the end of the gusset plate.

Fig. 9. Schematic view of bolted moment connection used for the optimisation process

Table 2 shows cross-sectional shapes of beam prototypes, Eurocode 3 design constraints, manufacturing limitations, and design variables including relative dimensions of the cross-sections, location of intermediate stiffeners, and angles of inclined lips. It should be mentioned that the manufacturing constraints were determined following consultation with the industrial advisor of this project.

The CFS beam with standard commercially available lipped-channel section (depth=260 mm, flange=79 mm, lip=16 mm, and plate thickness t=4 mm) is taken as a benchmark to assess the efficiency of the optimised solutions. In this study, five different beam cross-sectional shapes are selected; Beam ①: (back-to-back conventional lipped-channels); Beam ②: (beam ① with inclined lip); Beam ③: (beam ② + intermediate flange stiffeners); Beam ④: (beam ③+intermediate web stiffeners); and Beam ⑤: (back-to-back channels with folded-flanges).

The triangular intermediate web stiffeners consist of two 15 mm legs with an intersecting angle of 60°, and their locations are varied during the optimisation process to find their best positions within the cross-sectional web. The flange stiffeners are placed at the middle mainly for practicality reasons. The width of the flanges is also assumed to be at least 50 mm in order to connect trapezoidal decking or plywood boards to the beam by means of screws. The minimum feasible lip length for rolling or press-braking process is considered $c \geq 15$ mm. The web depth limit of $h \geq 200$ mm is also imposed to appropriately fit the selected bolt-group (170×170 mm) in the connection zone. In the adopted optimisation process, the plate thickness and the total coil width remain similar to the benchmark section to keep the material use of the cross-sections invariable. For the sections with web and flange stiffeners, their developed length is considered in the calculation of the total coil width.

In this study, the optimisation process is carried out on the CFS bolted moment connection based on either seismic performance indices: (I) energy dissipation capacity determined within the loading history up to drift ratio of 4% (i.e. SMF limit), or (II) ductility ratio calculated based on ASCE 41-17 [50] with the target rotation corresponding to 80% of peak moment in softening branch. The optimisation formulations are as follows:

Optimisation for energy dissipation capacity $E(X)$:

$$Max \quad E(X) \tag{5}$$

$$X_i^L \leq X_i \leq X_i^U, \qquad (i = 1, \dots, n) \tag{6}$$

Optimisation for ductility ratio $\mu(X)$:

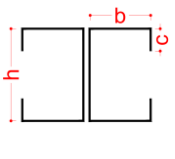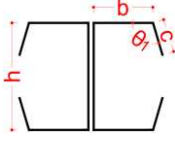$$Max \quad \mu(X) \tag{7}$$
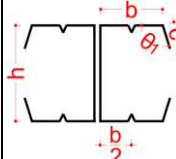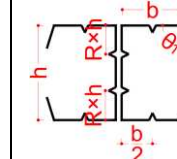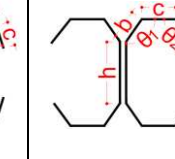
$$X_i^L \leq X_i \leq X_i^U, \qquad (i = 1, \dots, n) \tag{8}$$

where in the above equations X indicates a vector including cross-sectional design variables X_i listed in Table 2 with the lower bound X_i^L and upper bound X_i^U.

Table 2. Selected beam cross-sections, design variables and constraints

Prototypes	①	②	③	④	⑤
Cross-section					
Design variables (X_i)	$x_1=c/b$ $x_2=b/L$	$x_1=c/b$ $x_2=b/L$ $x_3=\theta_1$	$x_1=c/b$ $x_2=b/L$ $x_3=\theta_1$	$x_1=c/b$ $x_2=b/L$ $x_3=R$ $x_4=\theta_1$	$x_1=\theta_1$ $x_2=\theta_2$ $x_3=b$ $x_4=c$ $x_5=d$
EC3 design constraints	$0.2 \leq c/b \leq 0.6$ $b/t \leq 60$ $c/t \leq 50$ $h/t \leq 500$	$0.2 \leq c/b \leq 0.6$ $b/t \leq 60$ $c/t \leq 50$ $h/t \leq 500$ $\pi/4 \leq \theta_1 \leq 3/4\pi$	$0.2 \leq c/b \leq 0.6$ $b/t \leq 60$ $c/t \leq 50$ $h/t \leq 500$ $\pi/4 \leq \theta_1 \leq 3/4\pi$	$0.2 \leq c/b \leq 0.6$ $b/t \leq 60$ $c/t \leq 50$ $h/t \leq 500$ $\pi/4 \leq \theta_1 \leq 3/4\pi$ $0.1 \leq R \leq 0.4$	$h/t \leq 500$
Practical limitations (mm)	$c \geq 15$ $b \geq 50$ $h \geq 200$	$c \geq 15$ $b \geq 50$ $h \geq 200$	$c \geq 15$ $b \geq 50$ $h \geq 200$	$c \geq 15$ $b \geq 50$ $h \geq 200$	$7/12\pi \leq \theta_1 \leq 5/6\pi$ $\pi/4 \leq \theta_2 \leq 3/4\pi$ $b \leq 50;$ $c \leq 50;$ $d \geq 15$

5.2 Optimisation technique

A population-based stochastic optimisation technique, based on Particle Swarm Optimisation (PSO), was used to find the global optimised design solutions. An initial population of potential solutions (defined as a swarm of particles) is randomly selected. The particles then move in the problem space based on their own and neighbours' best performances. Unlike most conventional evolutionary optimisation techniques such as Genetic Algorithms (GA) [40, 55], PSO method does not require crossover or mutation operators. This usually results in a better computational efficiency especially for highly nonlinear optimisation problems [56, 57].

According to the PSO algorithm, a swarm contains N particles which possess different position ($\rho_i = \{\rho_{i1}, \rho_{i2}, \dots, \rho_{ij}, \dots, \rho_{iD}\}$) and velocity ($V_i = \{V_{i1}, V_{i2}, \dots, V_{ij}, \dots, V_{iD}\}$) in a D-dimensional search space. The initial position and velocity of particles are randomly generated to form a swarm, which is then spread out within the range of selected design variables ($X_i^L \leq X_i \leq X_i^U, (i = 1, \dots, n)$):

17

$$\rho_{ij}^0 = X_j^L + r_{ij}(X_j^U - X_j^L) \tag{9}$$

$$V_{ij}^0 = \frac{s_{ij}(X_j^U - X_j^L)}{\Delta t} \tag{10}$$

where matrices of r_{ij} and s_{ij} possess the components between 0 and 1. Subsequently, the particles fly through the search space to find the optimal solution. The velocity and position of the ith particle at k^{th} iteration are updated mathematically according to the following formulas:

$$V_i^{k+1} = wV_i^k + c_1r_1(P_{best,i}^k - \rho_i^k) + c_2r_2(G_{best}^k - \rho_i^k) \tag{11}$$

$$\rho_i^{k+1} = \rho_i^k + V_i^{k+1}\Delta t \tag{12}$$

where t is the selected time increment, and w is an inertial weight factor. The vectors $P_{best,i}^k = \{p_{i1}, p_{i2}, \dots, p_{ij}, \dots, p_{iD}\}$ and $G_{best}^k = \{g_1, g_2, \dots, g_D\}$ are, respectively, the best position of the ith particle over its history up to iteration k, and the position of the best particle in the swarm in iteration k. The cognitive parameter c_1 represents the level of confidence in the best position of the particle ($P_{best,i}$). The social parameter c_2 indicates the degree of confidence in the favourable position of the swarm. r_1 and r_2 are independent coefficients selected randomly between 0 and 1. To improve the convergence of the problem, the following recommendations made by Perez and Behdinan [58] were used:

$$0 < c_1 + c_2 < 4 \tag{13}$$

$$\frac{c_1 + c_2}{2} - 1 < w < 1 \tag{14}$$

In this study, the developed PSO algorithm was linked to GMNIA ABAQUS through scripting option which combines the functionality of the Graphical User Interface (GUI) of ABAQUS and the power of the Python object-oriented scripting language. The adopted optimisation process followed the following steps as also illustrated in the flowchart of Fig. 10:

(1) The experimentally validated FE model of a connection with the beam cross-sectional dimensions generated by PSO was built using Python script. A vertical displacement was applied at the beam tip, while the material properties, boundary conditions, and bolt modelling were taken the same as the validated model described in Section 3.

(2) The initial geometric imperfections of the CFS beam was generated by conducting an eigenvalue elastic linear BUCKLE analysis in ABAQUS and subsequently scaling the first buckling mode shape. The scale factor was determined based on the 50% cumulative distribution values for the measured local or distortional imperfections as reported by Schafer and Pekoz [48]. It should be noted that the local buckling was identified as the dominant failure mode in this type of connection [3, 11], hence imperfections magnitude was scaled to $0.34t$ (see Section 3).

(3) The standard "Static-General" analysis available in ABAQUS was performed and the required output data including the resisting moment, applied rotation, and dissipated energy ($E(X)$) were then extracted using the post-processing scripting in Python.

(4) The extracted moment-rotation output data were transferred to a MATLAB code for the calculation of ductility based on ASCE 41-17 [50].

(5) The values of energy dissipation capacity and ductility calculated in previous steps were imported to the PSO algorithm and a new particle was produced using Eqs. (11) and (12).

(6) This loop was repeated by starting a new iteration from step 1 until convergence was achieved or the maximum number of iteration was reached.

The population of the swarm was taken as 15 particles for beam prototypes ① to ③, while 20 particles were used for beam prototypes ④ and ⑤ due to their more complex shape (i.e. more design variables). The minimum and maximum inertial weight factors were selected as 0.4 and 0.95, respectively. To ensure all possible solutions were taken into account during the optimisation process, 250 iterations were considered as the maximum number of iterations.
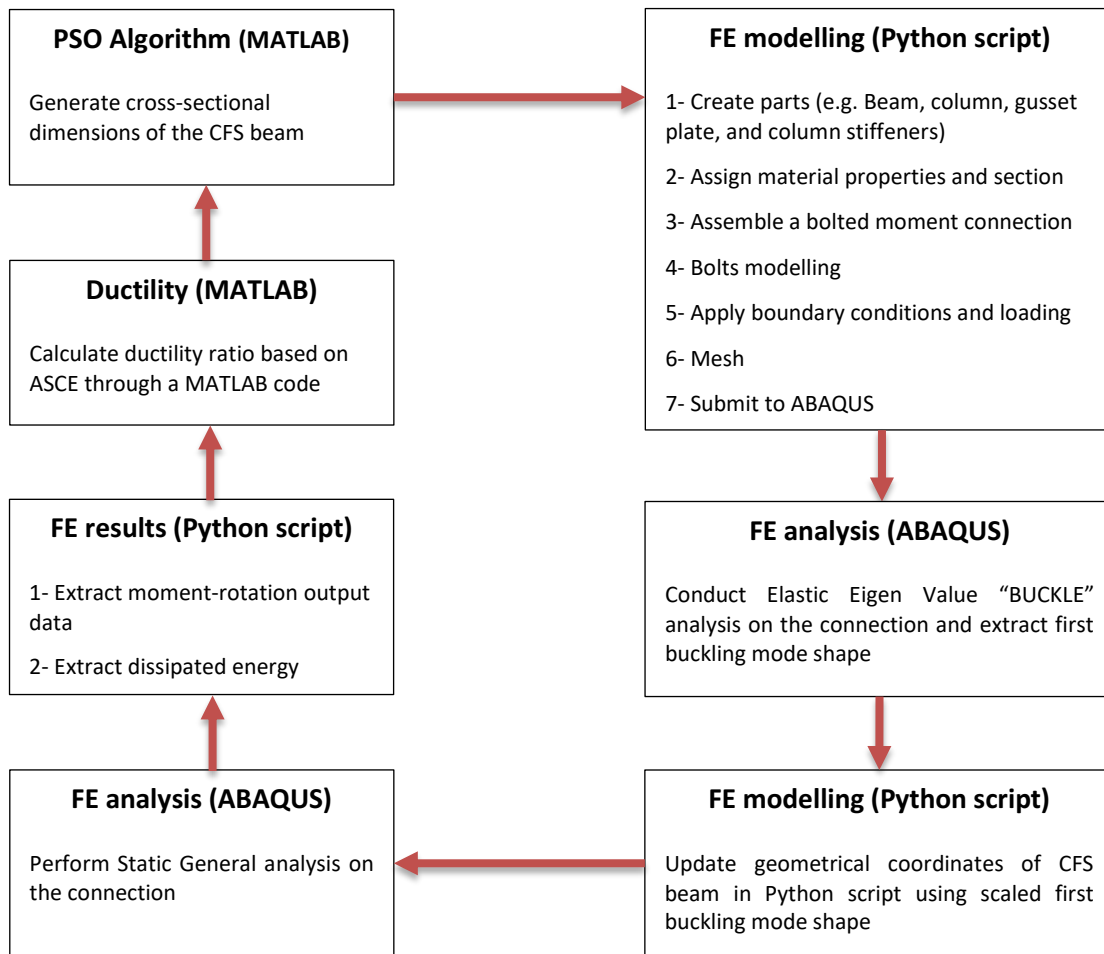
Fig. 10. Flowchart of optimisation process for maximum dissipated energy and ductility

6 Optimisation results

The developed optimisation methodology in this study required an extensive number of computations.

Therefore, the whole optimisation procedure was conducted on the University of Sheffield's High-

Performance Computing (HPC) cluster, which costs on average around 200 hours for each optimisation.

Each cross-section was optimised three times using random particles to ensure that the optimised

results are consistent. The maximum difference between the results obtained from the three runs was

always less than 2%, therefore the one with the highest value was selected.

6.1 Optimisation based on energy dissipation

The iteration history of optimisation process for the maximum energy dissipation of connections is shown in Fig. 11. It can be seen that the optimisation process for the connections with beam cross-sections ①, ②, and ③ converged to the best solution after around 60 iterations. For the more complex beam cross-sections ④ and ⑤, however, the convergence was achieved after only around 100 iterations due to more design variables leading to higher nonlinearity of the optimisation problem. These results confirm the adequacy of using 250 iterations for the optimisation process as mentioned before.

The cross-sectional dimensions of the optimised beams for maximum energy dissipation capacity are listed in Table 3. The results are compared with the energy dissipation and flexural strength of the benchmark connection (E_{ben}, $M_{u,ben}$) with the same amount of material (see Section 5). In general, it can be seen that the optimised connections with the highest energy dissipation capacity tend to provide a beam with minimum flanges width (herein 50 mm) and large web height (note that the total length of the cross-section is kept constant). This increase in the energy dissipation capacity of the connections is mainly attributed to (a) the delay in flanges buckling due to smaller width to thickness ratio, and (b) development of plastic zone in the beam web for a given drift ratio (4%) leading to higher peak moments.
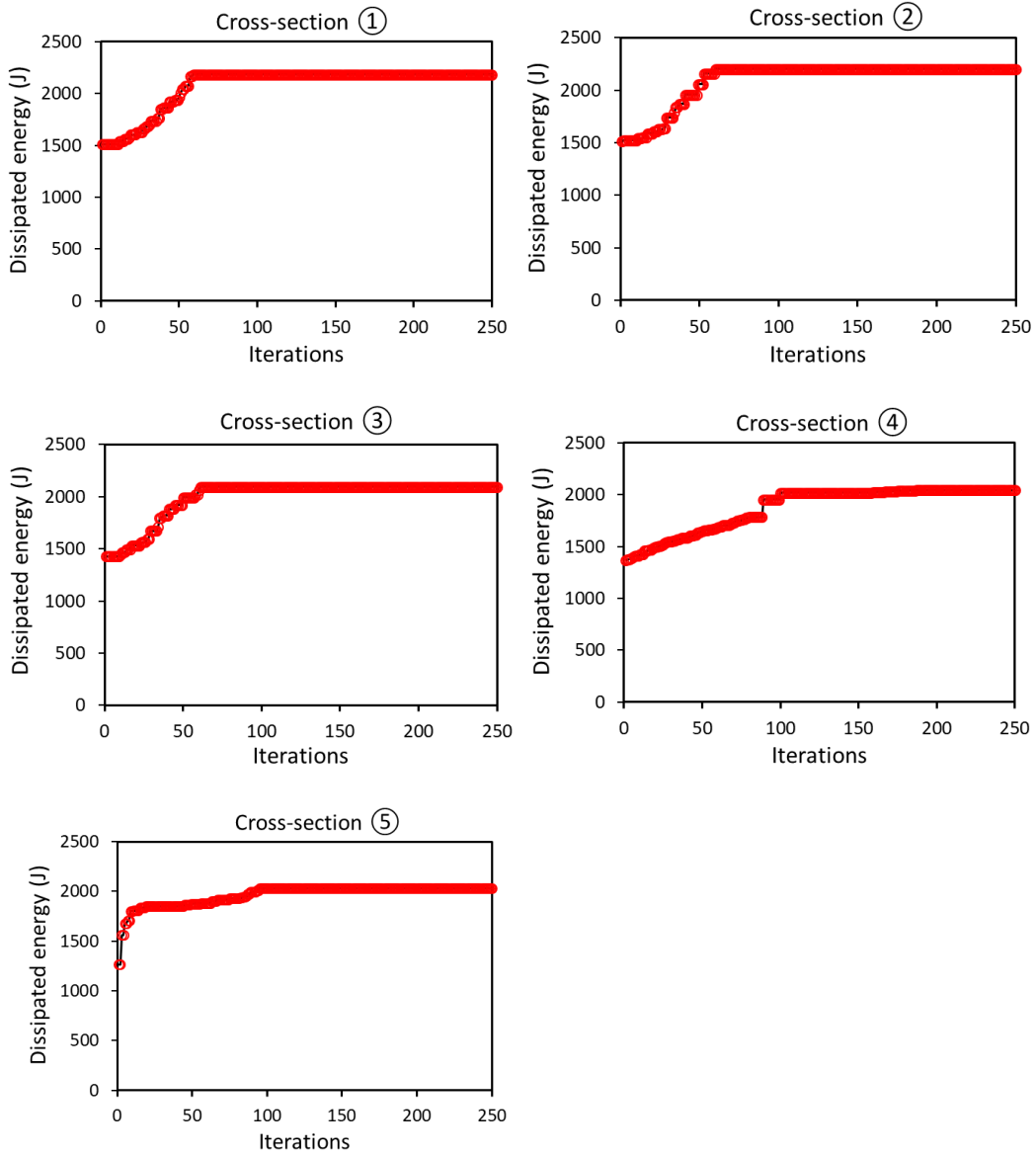
Fig. 11. Iteration history of optimisation process based on maximum dissipated energy for the connections with different beam cross-sections

Table 3. Dimensions, energy dissipation and moment capacity of optimised CFS bolted moment connections with different beam cross-sections

Beam section	h	b	c	d	R	θ_1	θ_2	E	$\dfrac{E}{E_{ben}}$	M_u	$\dfrac{M_u}{M_{u,ben}}$
	mm	mm	mm	mm		rad	rad	kJ		kN.m	
Benchmark	260	79	16					1.91	1.00	74.33	1
①	320	50	15					2.18	1.14	88.21	1.19
②	320	50	15			120		2.2	1.15	88.60	1.19
③	290	50	15			112		2.09	1.10	83.57	1.12
④	260	50	15		0.1	108		2.02	1.06	80.46	1.08
⑤	224	38	60	15		150	135	2.03	1.06	79.04	1.06

Fig. 12 compares the efficiency of different optimised beam shapes (①, ②, ③, ④, ⑤) used in the CFS bolted moment connection. Based on the results, the following considerations can be drawn:
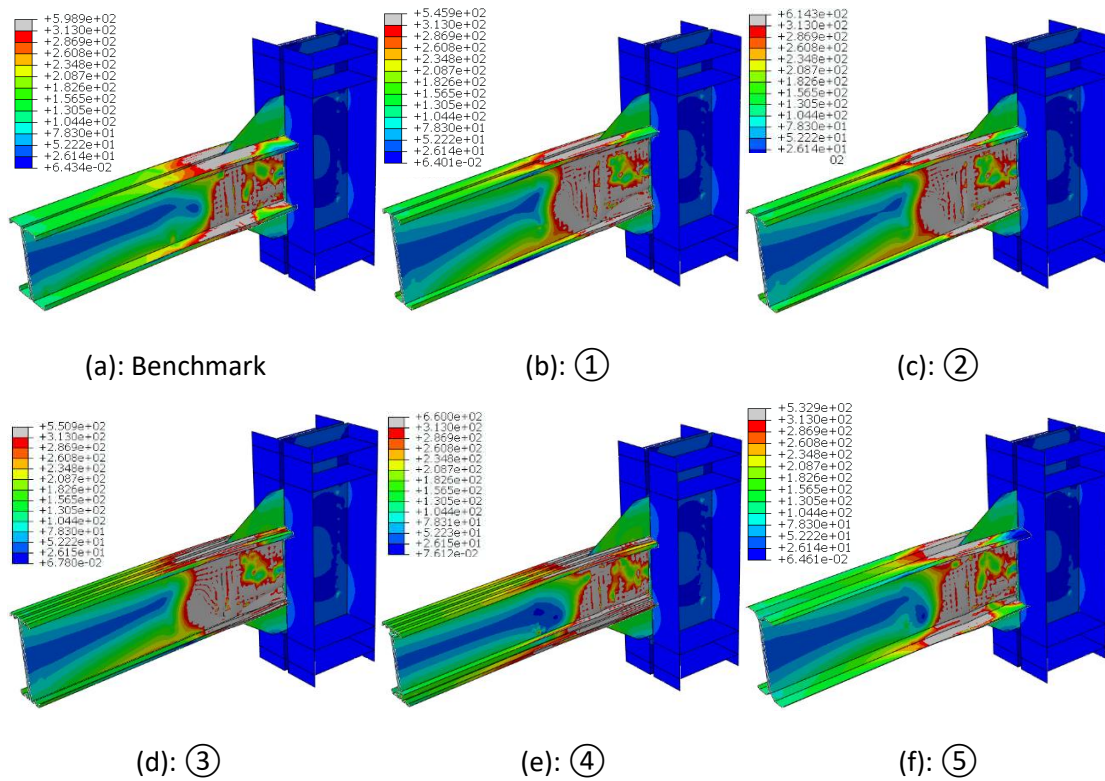
- The energy dissipation of the connection with the benchmark beam (E_{ben}) can be increased up to 14% by changing its relative dimensions (beam section ①). Consequently, the flexural strength of the benchmark connection ($M_{u,ben}$) is also improved by 19%.

- While the optimum lips' angle is calculated to be 120° in the connection with beam cross-section ②, generally releasing the lips' angle as an optimisation variable leads to a negligible increase in the energy dissipation capacity and strength of the connection.

- Incorporating intermediate stiffeners in the flanges (beam section ③) reduces the energy dissipation capacity and flexural strength of the connection by 4% and 5%, respectively, compared to optimised beam section ①. These reductions are exacerbated to 8% and 10% by adding combined intermediate stiffeners in the flanges and webs (beam section ④), as a result of the reduction in the cross-sectional web height. It should be noted that the stiffeners' legs are accounted for the total length of the cross-section, and therefore, the web height of the optimised beams ③ and ④ is less than that of optimised beam section ①. This can justify the results since decreasing the web height of the sections can generally reduce their energy dissipation capacity and flexural strength.

- A CFS connection with folded-flange beam section ⑤ provides approximately as much energy and strength as a connection with flange and web stiffeners beam section ④. The main reason is that the folded-flange beam section in this study had lower web slenderness compared to the other beam sections due to the imposed constraints for its constituent elements (listed in Table 2). It should be noted that, in general, folded-flange sections benefit from easer forming process and connection to typical floor systems compared to more complex sections such as curved flanges. This, therefore, demonstrates the efficiency of the beam with folded-flange section compared to those with intermediate stiffeners (sections ③ and ④).

23
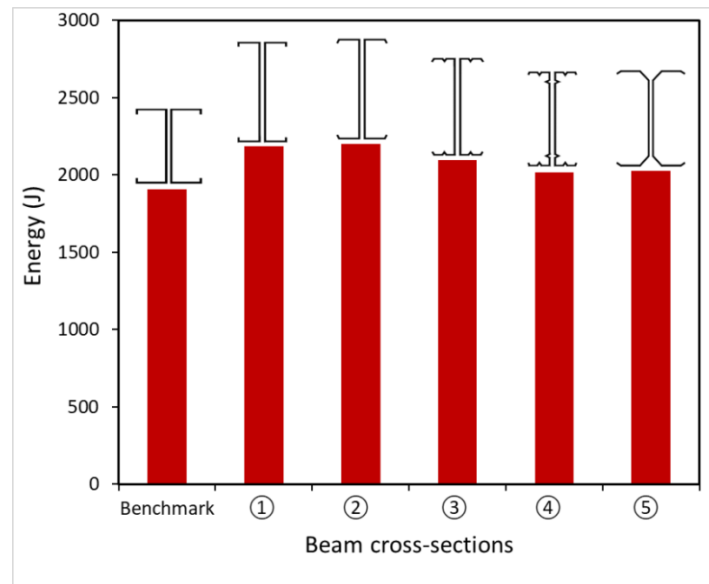
Fig. 12. Maximum energy dissipation provided by connections with optimised beams

The optimised connections in terms of energy dissipation capacity and their distribution of von Mises stresses are provided in Fig. 13. The main purpose of this figure is to illustrate the development of plasticity in the connection zone for different cross-sections. To clarify this, von Mises stress values larger than the yield stress f_y= 313 MPa are highlighted by the dark grey colour. It is seen that the connections with beam cross-sections ① and ② fail locally in the beam close to the first bolt line. However, the interaction of local and distortional buckling is dominant for the connections with beam cross-sections ③, ④, and ⑤. It is shown that the plastic zone in the connection with beam section ① is significantly more extended by simply optimising the relative dimensions of the benchmark beam, leading to higher energy dissipation capacity and flexural strength of the connection. While, optimising the lips' angle in beam section ② does not considerably affect the plastic zone, using connections with beam sections ③, ④, and ⑤ generally provides less plasticity compared to the connection with beam section ①. In general, these observations made from Fig. 13 are in agreement with the results presented in Table 3.

(a): Benchmark   (b): ①   (c): ②

(d): ③   (e): ④   (f): ⑤

Fig. 13. Von Mises stress contour of CFS bolted moment connection with standard and optimised beams based on maximum energy dissipation at 0.04 rad rotation

6.2 Optimisation based on ductility

Based on the results provided in Fig. 14, optimisation process based on ductility, in general, requires a higher number of iterations to find the optimised solution compared to the energy-based optimisation. It is shown that convergence is obtained after 80 iterations for the connections with beam sections ①, ②, and ③, while 150 iterations are needed for the connections with beam sections ④, and ⑤. Therefore, the selected maximum 250 iterations used in the optimisation process is sufficient.
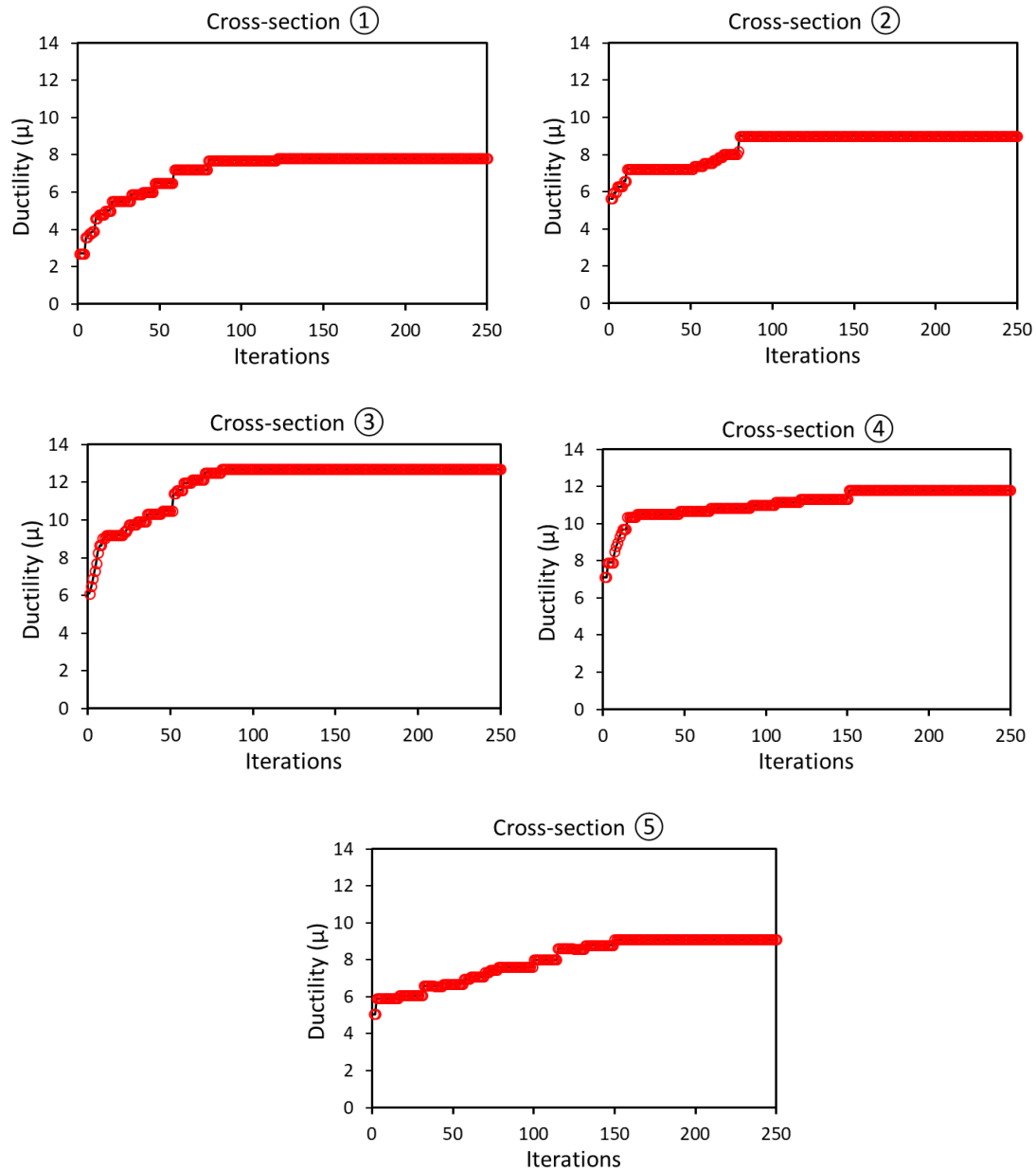
Fig. 14. Iteration history of optimisation process based on maximum ductility for the connections with different beam cross-sections

Table 4 lists the dimensions of optimised beam sections with the same steel coil width (450 mm) obtained from optimisation based on maximum ductility. The ductility and flexural strength of the benchmark connection ($\mu_{ben}, M_{u,ben}$) are also considered as a measure to investigate the efficiency of the optimised sections. As a general trend shown in Table 4, the adopted optimisation process enhances the ductility of the connections by reducing the height of the beam web (minimum 200 mm) and subsequently increasing the flange width and lip length. In this case, the local failure occurs in the flanges, which leads to a gradual drop in the moment-rotation curve.

Table 4. Dimensions, ductility and moment capacity of optimised CFS bolted moment connections with different beam cross-sections

Beam section	h mm	b mm	c mm	d mm	R	θ_1 rad	θ_2 rad	μ	$\dfrac{\mu}{\mu_{ben}}$	M_u kN.m	$\dfrac{M_u}{M_{u,ben}}$
Benchmark	260	79	16					4.3	1	74.33	1
①	200	78	47					7.6	1.77	58.60	0.79
②	200	78	47			104		9	2.09	58.39	0.79
③	200	69	41			104		12.7	2.95	60.47	0.81
④	200	59	36		0.4	95		11.8	2.74	63.44	0.85
⑤	200	30	65	30		110	68	9.1	2.12	60.25	0.81

Based on Table 4 and Fig. 15, the following remarks can be made:

- Ductility of the connection with the benchmark beam can be increased up to 77% by simply changing cross-sectional relative dimensions (section ①), however, its flexural capacity is reduced by 21%.

- By optimising the cross-sectional lips angle to 104˚ (section ②), the ductility ratio of the connection is increased up to 18%. However, the maximum moment capacity of the connection is not considerably affected.

- Unlike optimisation based on energy dissipation discussed in section 6.1, placing intermediate stiffeners in the flanges (section ③) or combined stiffeners in the flanges and web (section ④) can improve the ductility of the connection with optimised conventional beam (section ①) by 67% and 55%, respectively. Using intermediate stiffeners also slightly increases the flexural strength of the connection, mainly by delaying the stiffness degradation due to buckling.

- By using the optimised folded-flange beam (section ⑤), the ductility of the connection is increased by 20% compared to the connection with optimised conventional section (section ①), while no reduction is observed in the flexural strength of the connection.
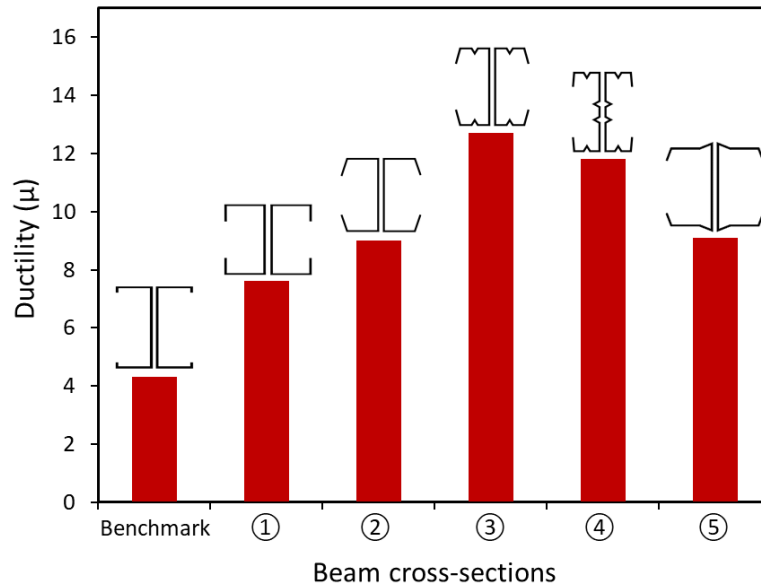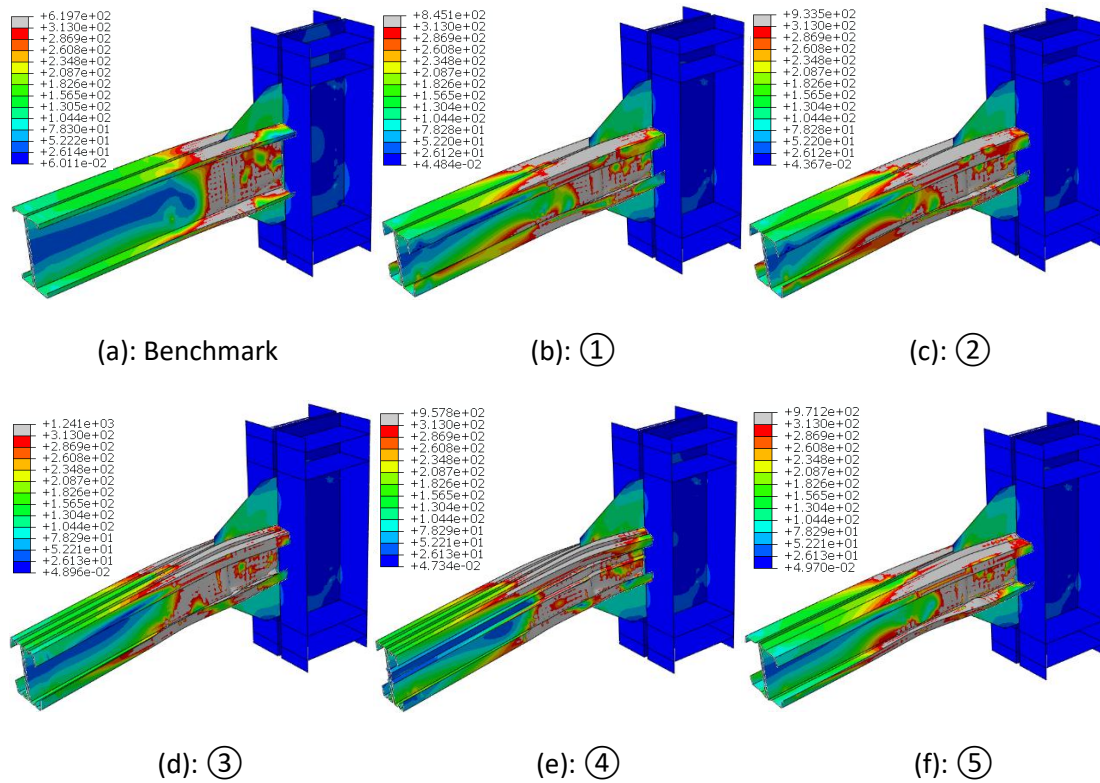
Fig. 15. Maximum ductility provided by connections with optimised beams

Fig. 16 shows the von Mises stress contour of the bolted moment connections with standard and optimised beams based on maximum ductility. The main purpose of this figure is to illustrate the development of plasticity in the connections with different cross-sections at their ultimate point (i.e. when its flexural strength drops by 20% from the peak moment). To clarify this, the regions with dark grey colour represent the stress values larger than the yield stress. It can be seen that, compared to the optimised connections based on energy dissipation, the plasticity is developed in a larger zone (especially in the flanges and lips) to maximise the ductility of the connection. Hence, optimised CFS bolted moment connections for ductility are capable to accommodate significant damage in the beam up to their ultimate point (i.e. rotation corresponding to a 20% drop from the peak moment).

As shown in Fig. 16, the failure of the benchmark connection with the standard beam is localised in the beam web mainly due to its large web slenderness; however, optimised connections with the lesser beam depth (200 mm) can develop plasticity and failure in both flanges and web. By optimising cross-sectional lips angle (section ②), plasticity is more distributed along the length of the CFS beam. Using intermediate stiffeners in the beam flanges (sections ③) results in a connection with the highest ductility due to a larger local failure zone in the flanges as well as the global buckling of the lips (distortional buckling of the section). Although the flanges of cross-section ④ are smaller than

28

cross-sections ①, ②, and ⑤, this cross-section is still able to provide more ductility due to the presence of intermediate flange stiffeners.

(a): Benchmark   (b): ①   (c): ②

(d): ③   (e): ④   (f): ⑤

Fig. 16. Von Mises stress contour of bolted moment connection with standard and optimised beams based on maximum ductility at 20% drop from maximum moment

It can be noted from the results that the proposed optimisation process based on maximum ductility could postpone the ultimate failure of the elements (i.e. higher ultimate rotation), while on the contrary, it reduced their flexural capacity. This indicates that, although the optimised sections always have higher ductility, they may exhibit slightly lower flexural capacity compared to the benchmark sections. It should be noted that if the capacity of the connection is of interest, the elements should be optimised by considering the maximum capacity of the connection as the optimisation target (e.g. [19]). Besides, the differences in the development of plasticity in the sections optimised based on ductility and energy dissipation capacity are mainly attributed to the definition of the ductility and energy dissipation as discussed before.

7 Effects of cyclic load on the optimised solution

As discussed in Section 5, performing optimisation on the detailed connection models (with nonlinear shell and fasteners elements) under cyclic load is highly computationally expensive, and therefore is not suitable for practical applications. In this section, the accuracy of using monotonic loading in the optimisation process as a more practical approach is assessed by investigating the effects of cyclic loading on the optimised solution. To this end, the connection with beam cross-section ① is optimised under the ANSI/AISC 341-16 [44] proposed cyclic loading (see Fig. 4). The University of Sheffield's High Performance Computing (HPC) cluster was used to solve this optimisation problem. The hysteretic behaviour of the optimised connections under cyclic loading optimised based on energy dissipation and ductility is also shown in Fig. 17. Table 5 lists the dimensions of the CFS beam section ① optimised based on maximum energy dissipation capacity and maximum ductility under cyclic load. Comparison between with these results with those obtained under monotonic load (Tables 3 and 4) indicates that, for both energy dissipation and ductility, the optimisation of the connections under cyclic load leads to the same optimised sections as those under monotonic load.

Table 5. Optimised dimensions of the CFS beam section ① in bolted moment connections under cyclic loading condition

Optimisation target	h (mm)	b (mm)	c (mm)
Energy dissipations	320	50	15
Ductility	200	78	47
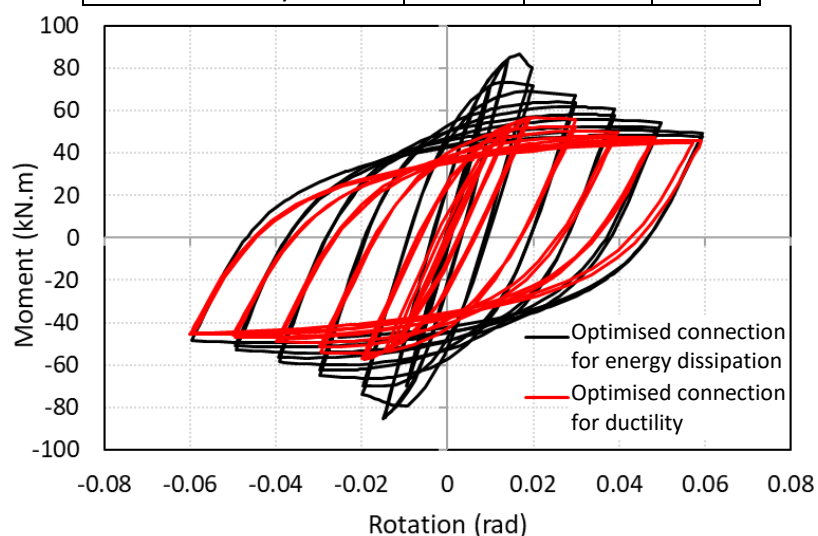
Fig. 17. Hysteretic behaviour of optimised connections for energy dissipation and ductility with beam cross-section ①

8 Efficiency of the optimised design solutions under cyclic load

One of the main issues associated with the use of CFS bolted moment connections in high seismic regions is their ability to develop the plastic hinge (i.e. moment hinge) and subsequently maintain the moment resistance under repeated rotations. It was shown in Section 3 that the post-peak behaviour and consequently the seismic characteristics of the CFS bolted moment connections can be very different under monotonic and cyclic load conditions. Therefore, in this section, the efficiency of the connections optimised under monotonic load (Sections 5 and 6) is investigated under cyclic load condition.

As shown in Table 6, energy dissipation (E_{cyc}) and ductility (μ_{cyc}) of the connections with optimised beam sections under cyclic load are increased by up to 20% and 164%, respectively, compared to those with standard beam sections. These observations are consistent with the general trend of the optimised results under monotonic load (see Section 6). This demonstrates again the efficiency of the proposed optimisation method, when the connections are subjected to cyclic load.

Table 6. Comparison between seismic characteristics of optimised connections under cyclic load

Beam section	Optimised connections for energy dissipation		Optimised connections for ductility	
	E_{cyc} kJ	$(\dfrac{E}{E_{ben}})_{cyc}$	μ_{cyc}	$(\dfrac{\mu}{\mu_{ben}})_{cyc}$
Benchmark	22.7	1	2.8	1
①	26.7	1.18	4.6	1.64
②	27.3	1.20	4.6	1.64
③	25.8	1.14	7.2	2.61
④	26.1	1.15	6.2	2.21
⑤	27	1.19	4.9	1.75

9 Summary and conclusions

This study presented an optimisation framework to develop more efficient CFS bolted moment connections with enhanced energy dissipation capacity and ductility. To achieve this, Particle Swarm Optimisation (PSO) algorithm was linked to GMNIA ABAQUS FE analysis using experimentally validated

Finite Element (FE) models of the connections by taking into account material non-linearity and geometrical imperfections. Five different CFS beam cross-sectional shapes were selected and their relative dimensions, location of intermediate stiffeners, and the inclination of the lip stiffeners were considered as key design variables. Based on the results, following conclusions can be drawn:

- By simply changing the relative dimensions of the lipped-channel beam section, the flexural strength, energy dissipation capacity, and ductility of the connection with the conventional lipped-channel beam section can be increased up to 19%, 14% and 77%, respectively. It was also shown that optimising the lips' angle only results in a negligible improvement in the structural performance of the connection. Therefore, for practical applications it is more cost effective to use channel sections with conventional 90^0 lips' angle.

- The adopted optimisation process enhanced the energy dissipation (up to 15%) of the connections generally by reducing the width of the beam flanges and subsequently increasing the web height. However, CFS beam elements in the optimised connections with the highest ductility tend to have minimum specified web height and larger flanges.

- Compared to the connection with the standard CFS beam section, the optimisation based on energy dissipation was generally accompanied by an improvement (up to 19%) in the flexural capacity of the connection, while the ductility based optimisation resulted in a lower flexural capacity (up to 21%).

- It was shown that using intermediate stiffeners in the beam section can improve both flexural strength and ductility of the connections by up to 67%. However, incorporating intermediate stiffeners in the beam section slightly (up to 8%) reduced the energy dissipation capacity of the connections compared to that with optimised lipped-channel beam section.

- Compared to the connection with optimised lipped-channel beam section, using optimised folded-flange beam section provided a more efficient connection in terms of ductility (up to 20%). However, optimised folded-flange beam section could not provide the same level of energy

32

dissipation capacity. This can be due to the lower web slenderness of the folded-flange beam section in this study imposed by the selected design constraints.

- For both energy dissipation and ductility, the optimisation of the CFS bolted moment connections under cyclic load leads to the same optimised sections obtained under monotonic load. It was also shown that the energy dissipation and ductility of the optimised connections under cyclic load follow the same general trend obtained for the optimised connections under monotonic load. This indicates that, to reduce the computational costs of the optimisation process, CFS connections can be efficiently optimised under monotonic load as suggested in this study.

10 Suggestions for future studies

The following suggestions can be adopted for further development of the present study in the future:

- The innovative optimisation procedure presented in this study can be further developed for a multi-criteria optimisation problem such as a simultaneous optimisation on both energy dissipation and ductility. While this can be a tedious task due to the heavy computational costs, the challenge would be to find an appropriate balance between ductility and energy dissipation for different seismic applications.

- The presented optimisation process can be replicated for a wider range of design variables, including different element slenderness, beam cross-sectional shapes (e.g. channels with intermediate stiffeners), bolt group length and configurations.

- The results of this study can be utilized at the frame level to assess the seismic performance of CFS moment-resisting frames using the proposed optimised CFS beams and bolted moment connections.

Acknowledgement

References

[1] G.J. Hancock, Design of Cold-formed Steel Structures (to AS/NZ 4600:2007), 4th ed ., Australian Steel Institute, North Sydney, Australia, 2007.

[2] J. Ye, S.M. Mojtabaei, I. Hajirasouliha, Local-flexural interactive buckling of standard and optimised cold-formed steel columns, Journal of Constructional Steel Research, 144 (2018) 106-118.

[3] A. Bagheri Sabbagh, M. Petkovski, K. Pilakoutas, R. Mirghaderi, Experimental work on cold-formed steel elements for earthquake resilient moment frame buildings, Engineering Structures, 42 (2012) 371-386.

[4] C.-L. Pan, M.-Y. Shan, Monotonic shear tests of cold-formed steel wall frames with sheathing, Thin-Walled Structures, 49 (2011) 363-370.

[5] A. Bagheri Sabbagh, Cold-formed steel elements for earthquake resistant moment frame buildings, PhD thesis, University of Sheffield, (2011).

[6] A. Bagheri Sabbagh, M. Petkovski, K. Pilakoutas, R. Mirghaderi, Ductile moment-resisting frames using cold-formed steel sections: An analytical investigation, Journal of Constructional Steel Research, 67 (2011) 634-646.

[7] D.P. McCrum, J. Simon, M. Grimes, B.M. Broderick, J.B.P. Lim, A.M. Wrzesien, Experimental cyclic performance of cold-formed steel bolted moment resisting frames, Engineering Structures, 181 (2019) 1-14.

[8] S.M. Mojtabaei, M.Z. Kabir, I. Hajirasouliha, M. Kargar, Analytical and experimental study on the seismic performance of cold-formed steel frames, Journal of Constructional Steel Research, 143 (2018) 18-31.

[9] H.B. Blum, K.J.R. Rasmussen, Experimental investigation of long-span cold-formed steel double channel portal frames, Journal of Constructional Steel Research, 155 (2019) 316-330.

[10] H.B. Blum, K.J.R. Rasmussen, Experimental and numerical study of connection effects in long-span cold-formed steel double channel portal frames, Journal of Constructional Steel Research, 155 (2019) 480-491.

[11] J.B.P. Lim, D.A. Nethercot, Ultimate strength of bolted moment-connections between cold-formed steel members, Thin Wall Structures, 41 (2003) 1019-1039.

[12] I. Elkersh, Experimental investigation of bolted cold formed steel frame apex connections under pure moment, Ain Shams Engineering Journal, 1 (2010) 11-20.

[13] B. Tshuma, M. Dundu, Internal eaves connections of double-bay cold-formed steel portal frames, Thin-Walled Structures, 119 (2017) 760-769.

[14] F. Öztürk, S. Pul, Experimental and numerical study on a full scale apex connection of cold-formed steel portal frames, Thin-Walled Structures, 94 (2015) 79-88.

[15] Rinchen, K.J.R. Rasmussen, Behaviour and modelling of connections in cold-formed steel single C-section portal frames, Thin-Walled Structures, 143 (2019) 106233.

[16] Rinchen, K.J.R. Rasmussen, H. Zhang, Design of cold-formed steel single C-section portal frames, Journal of Constructional Steel Research, 162 (2019) 105722.

[17] Rinchen, K.J.R. Rasmussen, Numerical modelling of cold-formed steel single C-section portal frames, Journal of Constructional Steel Research, 158 (2019) 143-155.

[18] R. Rinchen, K.J.R. Rasmussen, Experiments on Long-Span Cold-Formed Steel Single C-Section Portal Frames, Journal of Structural Engineering, 146 (2020) 04019187.

[19] D.T. Phan, S.M. Mojtabaei, I. Hajirasouliha, T.L. Lau, J.B.P. Lim, Design and Optimization of Cold-Formed Steel Sections in Bolted Moment Connections Considering Bimoment, Journal of Structural Engineering, 146 (2020) 04020153.

[20] S.M. Mojtabaei, J. Becque, I. Hajirasouliha, Local Buckling in Cold-Formed Steel Moment-Resisting Bolted Connections: Behavior, Capacity, and Design, Journal of Structural Engineering, 146 (2020) 04020167.

[21] N. Usefi, P. Sharafi, H. Ronagh, Numerical models for lateral behaviour analysis of cold-formed steel framed walls: State of the art, evaluation and challenges, Thin-Walled Structures, 138 (2019) 252-285.

[22] CEN, Eurocode 3: Design of Steel Structures. Part 1-1: General Rules and Rules for Buildings, in, Brussels: European Comittee for Standardization, (2005).

[23] M.H. Serror, E.M. Hassan, S.A. Mourad, Experimental study on the rotation capacity of cold-formed steel beams, J Constr Steel Res, 121 (2016) 216-228.

[24] Ž. Bučmys, A. Daniūnas, Analytical and experimental investigation of cold-formed steel beam-to-column bolted gusset-plate joints, Journal of Civil Engineering and Management, 21 (2015) 1061-1069.

[25] CEN, Eurocode 3: Design of Steel Structures. Part 1-8: Design of joints, in, Brussels: European Comittee for Standardization, (2005).

[26] A. Bagheri Sabbagh, M. Petkovski, K. Pilakoutas, R. Mirghaderi, Development of cold-formed steel elements for earthquake resistant moment frame buildings, Thin-Walled Structures, 53 (2012) 99-108.

[27] J. Ye, S.M. Mojtabaei, I. Hajirasouliha, K. Pilakoutas, Efficient design of cold-formed steel bolted-moment connections for earthquake resistant frames, Thin-Walled Structures, 150 (2020).

[28] J. Ye, S.M. Mojtabaei, I. Hajirasouliha, Seismic performance of cold-formed steel bolted moment connections with bolting friction-slip mechanism, Journal of Constructional Steel Research, 156 (2019) 122-136.

[29] A. Sato, C.-M. Uang, Seismic design procedure development for cold-formed steel–special bolted moment frames, Journal of Constructional Steel Research, 65 (2009) 860-868.

[30] AISI S100-12, North American specification for the design of cold-formed steel structural members, American Iron and Steel Institute (AISI), Washington, DC, USA, (2012).

[31] H. Parastesh, S. Mohammad Mojtabaei, H. Taji, I. Hajirasouliha, A. Bagheri Sabbagh, Constrained optimization of anti-symmetric cold-formed steel beam-column sections, Engineering Structures, 228 (2021) 111452.

[32] S.M. Mojtabaei, J. Becque, I. Hajirasouliha, Structural Size Optimization of Single and Built-Up Cold-Formed Steel Beam-Column Members, Journal of Structural Engineering, 147 (2021) 04021030.

[33] J. Ye, S.M. Mojtabaei, I. Hajirasouliha, P. Shepherd, K. Pilakoutas, Strength and deflection behaviour of cold-formed steel back-to-back channels, Engineering Structures, 177 (2018) 641-654.

[34] B. Wang, G.L. Bosco, B.P. Gilbert, H. Guan, L.H. Teh, Unconstrained shape optimisation of singly-symmetric and open cold-formed steel beams and beam-columns, Thin-Walled Structures, 104 (2016) 54-61.

[35] D.T. Phan, S.M. Mojtabaei, I. Hajirasouliha, J. Ye, J.B.P. Lim, Coupled element and structural level optimisation framework for cold-formed steel frames, Journal of Constructional Steel Research, (2019) 105867.

[36] J. Ye, J. Becque, I. Hajirasouliha, S.M. Mojtabaei, J.B.P. Lim, Development of optimum cold-formed steel sections for maximum energy dissipation in uniaxial bending, Engineering Structures, 161 (2018) 55-67.

[37] S.M. Mojtabaei, J. Ye, I. Hajirasouliha, Development of optimum cold-formed steel beams for serviceability and ultimate limit states using Big Bang-Big Crunch optimisation, Engineering Structures, 195 (2019) 172-181.

[38] Abaqus/CAE User's Manual, version 6.14-2, USA, (2014).

[39] Mathworks, Matlab R2015b, Mathworks Inc., (2015).

[40] Kennedy J, Eberhart R, Particle swarm optimization, Neural Networks, 1995. Proceedings., IEEE International Conference on, IEEE, 1995, pp. 1942–1948.

[41] CEN, EN 1998-1, Design of Structures for Earthquake Resistance - Part 1: General Rules, Seismic Actions and Rules for Buildings, (2005).

[42] AISI S400-15, North American Standard for seismic Design of Cold-Formed Steel Structural Systems, American Iron and Steel Institute (AISI), Washington, DC, USA, (2015).

[43] C.M. Uang, A. Sato, J.K. Hong, K. Wood, Cyclic Testing and Modeling of Cold-Formed Steel Special Bolted Moment Frame Connections, Journal of Structural Engineering, 136 (2010) 953-960.

[44] ANSI/AISC 341-16, Seismic provisions for structural steel buildings, American Institute of Steel Construction (AISC), (2016).

[45] S.M. Mojtabaei, J. Becque, I. Hajirasouliha, Behavior and Design of Cold-Formed Steel Bolted Connections Subjected to Combined Actions, Journal of Structural Engineering, 147 (2021) 04021013.

[46] AS/NZS 4600, Coldformed steel structures, Homebush, Australia, Standards Australia/Standards New Zealand (SA/SNZ), (2018).

[47] N. Usefi, H. Ronagh, P. Sharafi, Numerical modelling and design of hybrid cold-formed steel wall panels, Thin-Walled Structures, 157 (2020) 107084.

[48] B.W. Schafer, T. Peköz, Computational modeling of cold-formed steel: characterizing geometric imperfections and residual stresses, Journal of Constructional Steel Research, 47 (1998) 193-210.

[49] A.C. Walker, Design and analysis of cold-formed sections, Halsted Press, 1975.

[50] ASCE/SEI 41-17, Seismic Evaluation and Retrofit of Existing Buildings, American Society of Civil Engineers (ASCE), (2017).

[51] C.M. Uang, Establishing R (or Rw) and Cd factors for building seismic provisions, Journal of Structural Engineering, 117(1) (1991) 19–28.

[52] E.F. Gad, A.M. Chandler, C.F. Duffield, G.L. Hutchinson, Earthquake ductility and overstreng thin residential structures, Structural Engineering and Mechanics, 8(4) (1999) 361-382.

[53] CEN, Eurocode 3: design of steel structures, part 1.3: general rules—supplementary rules for cold formed members and sheeting, in, Brussels: European Comittee for Standardization, (2005).

[54] CEN, Eurocode 3: Design of steel structures, Part 1-5: Plated structural elements, in, Brussels: European Comittee for Standardization, (2006).

[55] J. Ye, I. Hajirasouliha, J. Becque, K. Pilakoutas, Development of more efficient cold-formed steel channel sections in bending, Thin-Walled Structures, 101 (2016) 1-13.

[56] R. Hassan, B. Cohanim, O. De Weck, G. Venter, A comparison of particle swarm optimization and the genetic algorithm, in: Proceedings of the 1st AIAA multidisciplinary design optimization specialist conference, 2005, pp. 18-21.

[57] S. Jeong, S. Hasegawa, K. Shimoyama, S. Obayashi, Development and investigation of efficient GA/PSO-hybrid algorithm applicable to real-world design optimization, Computational Intelligence Magazine, IEEE, 4 (2009) 36-44.

[58] R.E. Perez, K. Behdinan, Particle swarm approach for structural design optimization, Comput Struct, 85 (2007) 1579-1588.